doi:10.3788/gzxb20124105.0558

Numerical Analysis of SPP Maskless Interference Lithography System

DONG Qi-ming, GUO Xiao-wei

(*School of Optoelectronic Information, University of Electronic Science and Technology, Chengdu* 610054, *China*)

Abstract: The use of the surface plasmon ploritons(SPPs) instead of photons as the exposure source can pattern nanoscale feature size by its near field enhancement effects. In this paper, we numerically explore the parameter spaces in prism-based SPP lithography system. The calculation principles and methods are given out. Results show that high refractive indices of prism, low thickness of silver film, appropriate incidence wavelength and the refractive indices of resist contribute to optimal interference image with high expore depth and contrast. When chosing 40 nm silver film at 431 nm incidence wavelength, exposure depth achieves 200 nm, and fringes period is 110 mm. The numerical results offer theoretical support for the arrangement of the experimental setup.

Key words: Interference lithography; Surface plasmon plortiton; Kretschmann structure

CLCN: TN305.7 **Document Code**: A **Article ID**: 1004-4213(2012)05-0558-7

0 Introduction

There is a growing interest in exploring new nanolithography techniques with high efficiency, low cost and large-area fabrication to fabricate nanoscale devices for nanotechnology applications. Conventional photolithography has remained a useful microfabrication technology because of its ease of repetition and suitability for large-area fabrication[1]. The diffraction limit, however, restricts the fabrication scale of photolithography[2]. Potential solutions that have actually been pursued require increasingly shorter illumination wavelengths for replicating smaller structures. It is becoming more difficult and complicated to use the short optical wavelengths to reach the desired feature sizes. Other methods such as electron beam lithography[3], ion beam lithography[4], scanning probe lithography[5], nanoimprint lithography(NIL)[6], and evanescent near-field optical lithography (ENFOL)[7] have been developed in order to achieve nanometer-scale features. As we know, the former three techniques need scanning and accordingly are highly inefficient. In NIL, the leveling of the imprint template and the substrate during the printing process, which determines the uniformity of the imprint result, is a challenging issue of this method. ENFOL have the potential to produce subwavelength structures with high efficiency, but it encounters the fact that the evanescent field decays rapidly through the aperture, thus attenuating the transmission intensity at the exit plane and limiting the exposure distance to the scale of a few tens of nanometers from the mask.

In recent years, the use of surface-plasmon polaritons (SPPs) instead of photons as an exposure source was rapidly developed to fabricate nanoscale structures. SPPs are characterized by its near field enhancement so that SPP-based lithography can greatly extend exposure depth and improve pattern contrast. Grating-assisted SPP interference, such as SPP resonant interference nanolithography[8] and SPP-assisted interference nanolithography[9], achieved a sub-100nm interference pattern. The techniques, however, are necessary to fabricate a metal grating with a very fine period and only suitable for small-area interference. To avoid the fabrication of the metal grating, a prism-based SPP maskless interference lithography was proposed in 2006[10], which promises good lithography performance. The approach offers potential to achieve sub-65nm and even sub-32nm feature sizes[11-15].

However, the structure parameters are always not ideal in a real system. One wants to know how much influence the parameter variations have on the pattern resolution and what variations of the parameters are allowed to obtain an effective interference. Thus, it is necessary to explore the

Foundation item: The National Natural Science Foundation of China (No. 60906052)

First author: DONG Qi-ming (1986 —), male, M. S. degree candidate, mainly focuses on micro and nanofabrication, micro and nano photonics. Email: dongjiao003@163.com

Corresponding author (Contact author): GUO Xiao-wei(1975—), male, associate professor, mainly focuses on micro and nanofabrication, micro and nano photonics, photo-electronic signal processing, integrated optics and fiber sensor. Email: gxw@uestc.edu.cn

Received date: 2011-12-05 **Revised date**: 2012-01-10

parameter spaces.

1 SPP maskless interference lithography system

The SPP maskless interference lithography system is shown in Fig. 1. A p-polarized laser is divided into two beams by a grating splitter, and then goes into the prism-based multilayer system. Under a given condition, the metal film can exhibit collective electron oscillations known as SPPs which are charge density waves that are characterized by intense electromagnetic fields confined to the metallic surface. If the metal layer

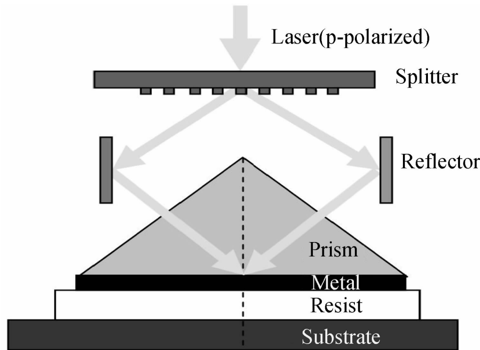

Fig. 1 Schematic for SPP maskless interference lithography system

is sufficiently thin, plasma waves at both metal interfaces are coupled, resulting in symmetric and antisymmetric SPPs. When the thickness h of metal film, dielectric constant ε_1, ε_2, ε_3 of medium above, inside, below the metal film are specified, the coupling equation is shown as follows[16]

$$\tanh(S_2h)(\varepsilon_1\varepsilon_3S_2^2+\varepsilon_2^2S_1S_3)+(\varepsilon_1\varepsilon_2S_2S_3+\varepsilon_2\varepsilon_3S_1S_2)=0$$

$$S_j^2=k^2-\varepsilon_jk_0^2 \quad (j=1,2,3) \quad (1)$$

in which k_0 is the value of the wave vector of illumination light, k is the value of the wave vector of SPP.

For a thin metal film, however, the wave vector of SPP is always larger than that of the light line[17]. The momentum transfer of an optical wave to the resultant SPP is enhanced by prism-coupling method. When SPP resonance occurs, the horizontal direction component k_x of incident optical wave vector must be equal to k_{sp} on the surface of metal film. The relation between k_x and k_{sp} is

$$k_x=k_0n_p\sin\theta_i=k_{sp} \quad (2)$$

where n_p is the refractive index of the prism and θ_i is the incidence angle of the optical wave to excite the plasma waves, namely resonance angle. Under resonance conditions, the light energy is transferred to the resultant SPPs forming a large near-field enhancement. If the resonance frequency falls within the sensitivity range of a photoresist, the field enhancement can be used to locally expose the thin resist layer.

2 Calculation and simulation method

2.1 Calculation of the resonance angle

For a given structure, it is vital to find the resonance angle for the excitation of the SPPs. The resonance angle can be found from the curve of the reflectance as a function of the incidence angle. The incidence angle at the reflectance minimum is the resonance angle. The reflectance of the prism-metal film-resist-substrate system can be written as[17]

$$R_{1234}=\frac{r_{12}+R_{234}\exp(\mathrm{i}2k_{2z}d_2)}{1+r_{12}R_{234}\exp(\mathrm{i}2k_{2z}d_2)} \quad (3)$$

$$R_{234}=\frac{r_{23}+R_{34}\exp(\mathrm{i}2k_{3z}d_3)}{1+r_{23}R_{34}\exp(\mathrm{i}2k_{3z}d_3)} \quad (4)$$

Here r_{ij} is the Fresnel reflection coefficient for p-polarized light and k_{iz} is the normal component of the wave vector, they are given by

$$r_{ij}=\frac{\sqrt{\varepsilon_j}\cos\theta_i-\sqrt{\varepsilon_i}\cos\theta_j}{\sqrt{\varepsilon_j}\cos\theta_i+\sqrt{\varepsilon_i}\cos\theta_j} \quad (5)$$

$$k_{iz}=\frac{\omega}{c}(\varepsilon_i-\varepsilon_1\sin^2\theta_1)^{1/2} \quad (6)$$

The subscripts $i, j=1\sim4$ refer to the prism, the metal, the resist, and the substrate, respectively, where ε_i and d_i are the dielectric constant and the thickness of the appropriate medium. The angle of the wave vector in each medium is given by θ_i, and ω and c are the angular frequency of the incident wave and the speed of light, respectively.

2.2 Simulation of the electromagnetic propagation in a metal structure

To simulate the interference pattern, finite-difference time domain (FDTD) technique is used. But the dielectric constant of the metal at optical frequencies is complex numbers because of the absorption, and in most cases the real part of the dielectric constants are negative, this makes the standard time iteration scheme of FDTD method unstable. The metal Drude model is expressed by

$$\varepsilon_D(\omega)=\varepsilon_\infty-\frac{\omega_D^2}{\omega^2+\mathrm{i}\Gamma_D\omega} \quad (7)$$

With ε_∞ the relative permittivity at infinite frequency, ω the angular frequency of the optical field, ω_D the bulk plasma angular frequency, and Γ_D the average time between subsequent electron collisions. To overcome the unstable problem, a current density term[18] is used as shown below

$$\varepsilon_{eff}\frac{\partial E_x}{\partial t}=\frac{\partial H_z}{\partial y}-J_x$$

$$
\begin{aligned}
&\varepsilon_{\mathrm{eff}}\frac{\partial E_y}{\partial t}=-\frac{\partial H_z}{\partial x}-J_y\\
&\mu_0\ \frac{\partial H_z}{\partial t}=-\left(\frac{\partial E_y}{\partial x}-\frac{\partial E_x}{\partial y}\right)\\
&\frac{\partial J_x}{\partial t}=\alpha J_x+\beta E_x\\
&\frac{\partial J_y}{\partial t}=\alpha J_y+\beta E_y
\end{aligned}
\tag{8}
$$

where $\varepsilon_{\mathrm{eff}}$, α and β are related to ε_∞, Γ_{D} and ω_{D} in Drude model as

$$
\begin{aligned}
&\varepsilon_{\mathrm{eff}}=\varepsilon_0\varepsilon_\infty\\
&\alpha=-\Gamma_{\mathrm{D}}\\
&\beta=\varepsilon_0\varepsilon_{\mathrm{D}}^2
\end{aligned}
\tag{9}
$$

3 Numerical analysis and discussion

According to the coupling equation (1), the wave vector of SPPs depends on the thickness of the metal film and the dielectric constants of the three materials. The metal dielectric constant is a frequency-dependent value. Therefore, the pattern resolution is actually determined by the incidence wavelength, the thickness of the metal film and the refractive indices of the prism and the resist. In the following analysis, the dependence of the resolution on one of them is investigated separately by keeping others constant.

3.1 The interference pattern

The reflectance as a function of the incidence angle is plotted in Fig. 2(a). The refractive index of the prism and photoresist are 1.943 25 (SF59 coupling prism) and 1.53 (AZ9200 from AZ Electronic Material), respectively, and the wavelength used is 431 nm. The metal layer is chosen to be silver because its plasmon frequency is located at UV range and its frequency-dependent dielectric constant is $-6.059\ 8+0.197\ 0i$ at 431 nm wavelength[19]. The silver thickness is 40 nm. It can be seen that the resonance angle is 79.5°. The interference pattern on the photoresist is shown in Fig. 2(b). We observe that the period of interference pattern is about 110 nm, which agrees well with the theoretical result $\Lambda=\lambda/2(n_{\mathrm{p}}\sin\theta_{\mathrm{sp}})=113$ nm. To determine the quality of the interference pattern, exposure depth and pattern contrast are adopted as evaluation factors. The normalized electric field intensity, $I=|E|^2/|E_0|^2$, is used to determine the exposure depth, where $|E_0|^2$ is the incident intensity. From Fig. 2(c), it can be seen that the exposure depth is about 200 nm. The contrast $V=(t^2-1)/(t^2+1)$ is defined by Ref. [10], where t is the ratio of E_z/E_x. Fig. 2(d) shows the interference lithography can obtain around 0.75 fringe visibility which is far beyond 0.2 that is the contrast threshold required in conventional lithography.

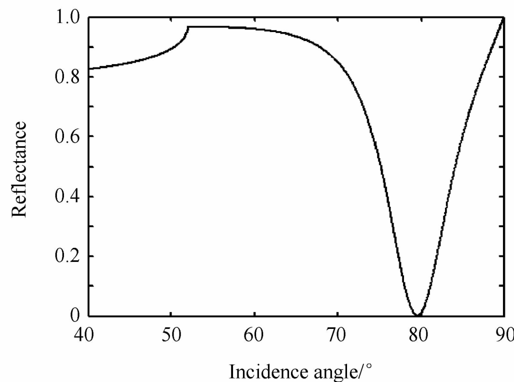

(a) Reflectance vs incidence angle

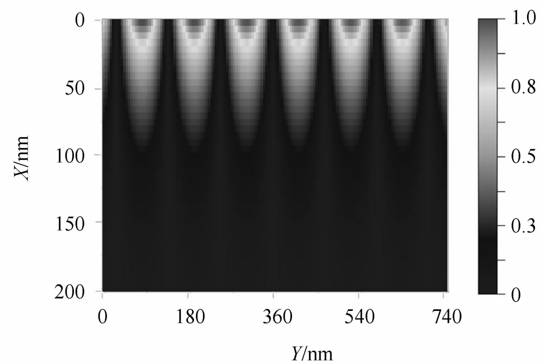

(b) Interference pattern

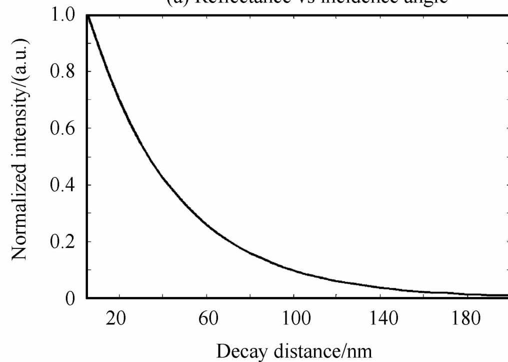

(c) Normalized intensity vs decay distance

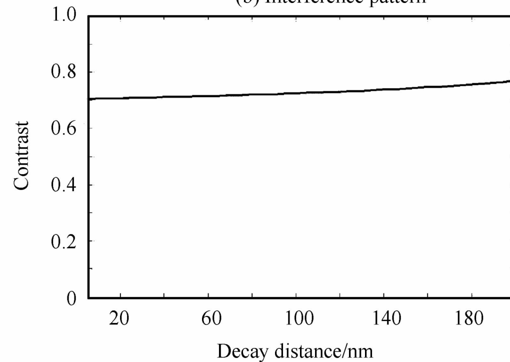

(d) Contrast vs decay distance

Fig. 2 The reflectance of the multiple films as a function of incident angle, the interference pattern, and the normalized intensity and contrast as a function of decay distance

3.2 The parameter spaces

3.2.1 *Incidence wavelength*

Fig. 3 illustrates the effects of incidence wavelength variations on the interference pattern. The incidence wavelength varies from 400 nm to 700 nm covering whole visible light range. From Fig. 3(a), it is observed that the resonance angle dramatically decreases with the increase of incidence wavelength. The long wavelength will arouse the resonance angle close to the total internal reflectance angle in the system without metal film. Fig. 3(b) gives out the relation between the period of the interference pattern and the incidence wavelength. The period almost is a linear function of incidence wavelength and the period changes from 110 nm to 220 nm in the wavelength range. However, different wavelengths achieve different exposure depths as shown in Fig. 3(c). The largest exposure depth occurs at the wavelength of 431 nm. At the wavelengths smaller than 431 nm, the exposure depth decreases quickly. On the other hand, the exposure depth varies slowly when the wavelength is greater than 431 nm. If 40nm is taken as the threshold of resist thickness for existing spinning technology, only incidence wavelengths greater than 414 nm can be allowed to illuminate the lithography system for obtaining effective interferences. Considering even contrast dependence of decay distance as depicted in Fig. 2(d), we use the contrast at the end of exposure depth to represent the contrast of the interference pattern. Fig. 3(d) shows the contrast as a function of the incidence wavelength. It can be seen that all the contrasts are high enough for lithography purpose.

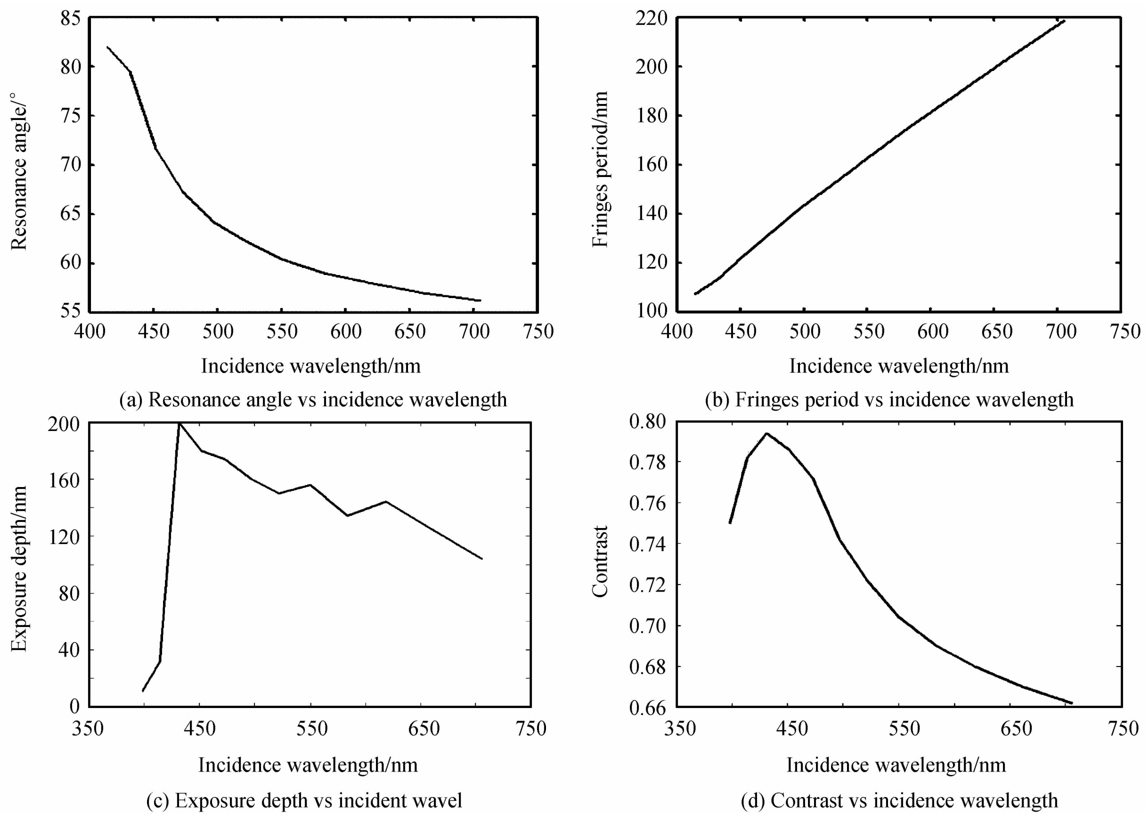

Fig. 3　The resonance angle, the period, exposure depth and contrast as a function of incidence wavelength

3.2.2 *The thickness of the metal film*

The effects of the silver thickness variations are described in Fig. 4. In Fig. 4 (a), the resonance angle increases with increasing the thickness of the silver film. It means using thick silver film achieves high spatial resolution at a given wavelength, which differs from the result in the reference[20]. But the difference is very limited(see Fig. 4(b)). The period varies only 12 nm when the thickness increases from 15 nm to 65 nm. Fig. 4(c) gives out the exposure depths at different thicknesses. The exposure depth is very sensitive to the silver thickness. The exposure depth is about 500 nm at 20 nm silver thickness, but it falls down to 50 nm when the silver thickness increases to 60 nm. Fig. 4(d) shows the contrast as a function of the metal thickness. There is an interesting phenomenon that the metal thickness also affects the contrast greatly, which indicates that the coupling of the SPPs between two

interfaces strongly depends on the metal thickness. For thin metal film, evanescent wave penetrates deeply into the metal film so strong resonance is obtained. On the contrary, thick metal film blocks the SPP coupling between two interfaces so that bad contrast is formed. With the continuous increase of the metal thickness, the exposure depth and contrast will become unavailable. Therefore, silver thickness should be limited within 60 nm.

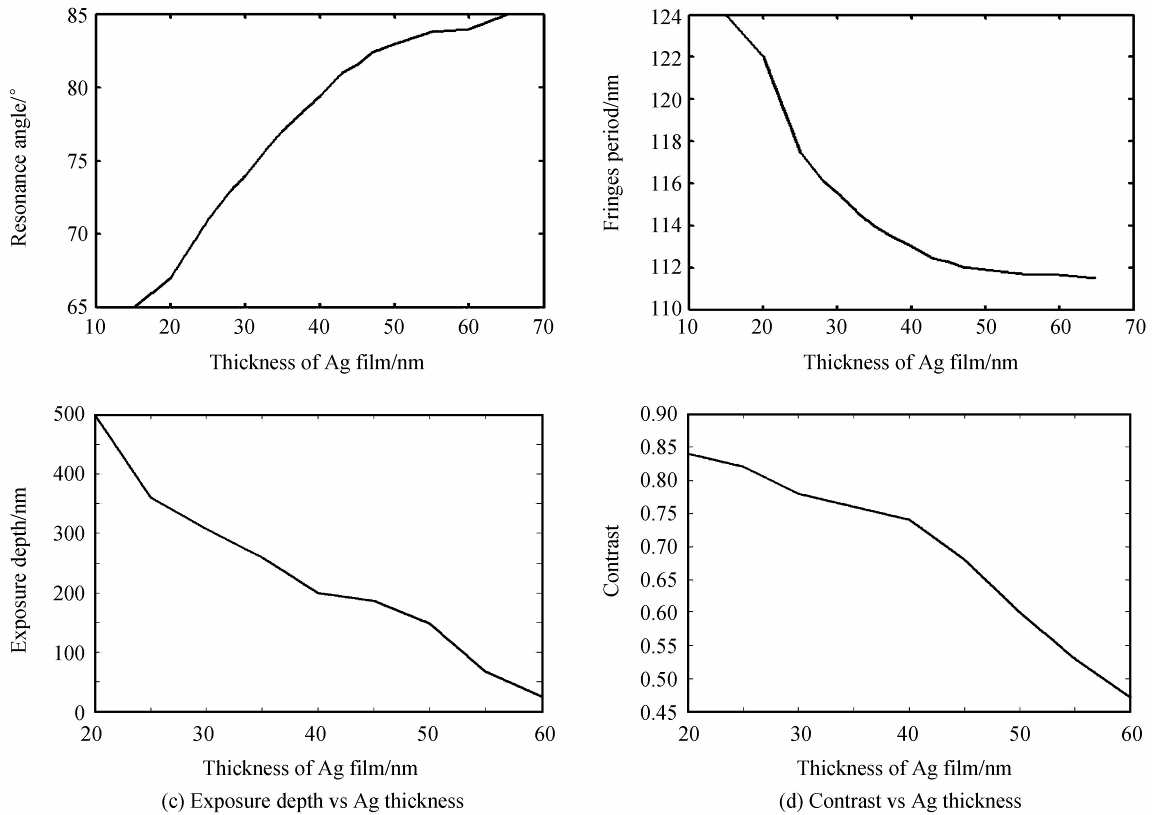

Fig. 4 The resonance angle, the period, exposure depth and contrast as a function of the silver thickness

3.2.3 *The refractive index of the prism*

Fig. 5 gives out the interference results at different refractive indices of the prism. In Fig. 5 (a), it can be seen that the resonance angle increases firstly with the increase of the prism refractive index, and then attains peak at the refractive index of 1.9, and finally decreases as the refractive index increases. According to equation (2), the wave vector of the SPP depends on not only the resonance angle but also the refractive index of the prism so it needs further analysis. Fig. 5 (b) plots the period dependence of the refractive index. The period changes less than 5nm in entire refractive index range, which shows that the prism refractive index has small influence on the resolution. The exposure depth as a function of the refractive index is shown in Fig. 5 (c). It is obvious that high prism index generates large exposure depth. This is because large difference of the refractive index between the prism and the resist results in small resonance angle which contributes to large penetration depth of the

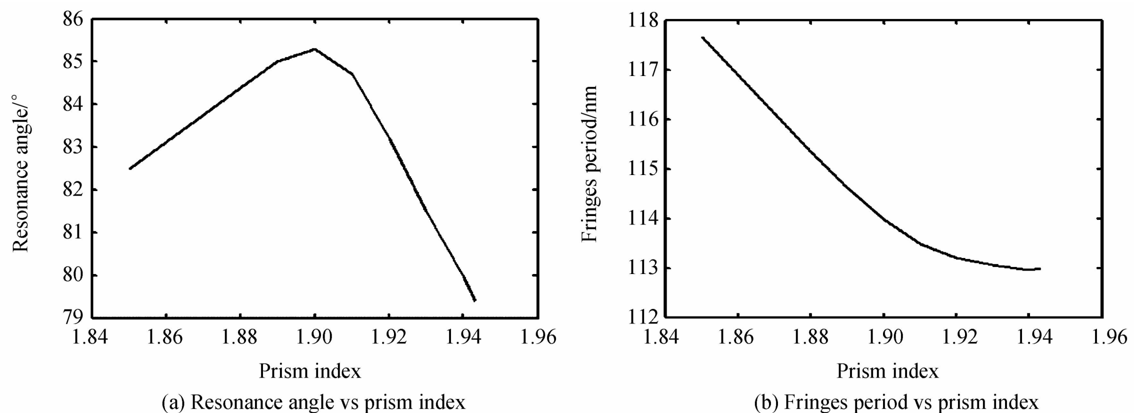

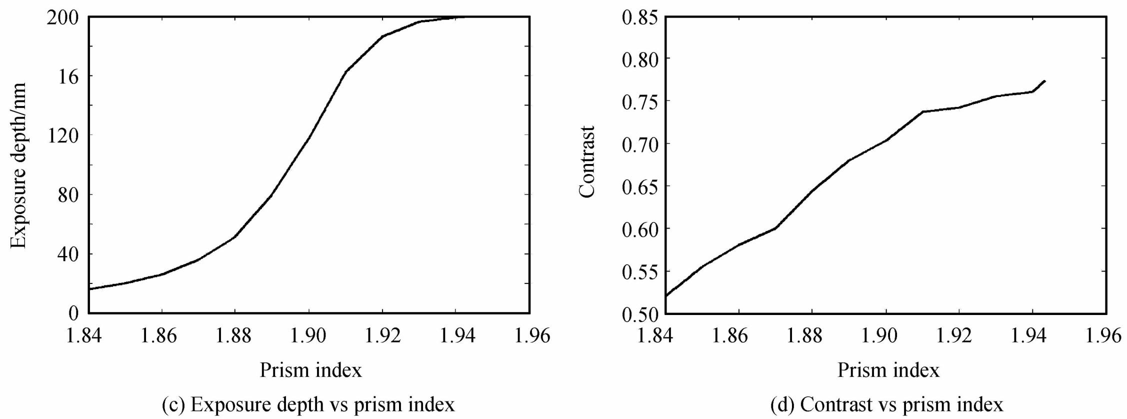

(c) Exposure depth vs prism index (d) Contrast vs prism index

Fig. 5 The resonance angle, the period, exposure depth and contrast as a function of the prism index

evanescent wave. The deep penetration easily excites SPP resonance. Fig. 5 (d) shows the pattern contrast as a function of the prism index. It is seen as with the metal thickness the prism index also affects the contrast greatly. To achieve more than 50 nm exposure depth, the refractive index of the prism should be chosen over 1.88.

3.2.4 *The refractive index of the resist*

Different SPP wave vectors generally need the use of different resists. Fig. 6 describes the effects of the resist variations on the resolution. In Fig. 6 (a), the resolution is not a linear function of the refractive index of the resist. The resonance angle firstly increases with the increase of the refractive index of the resist and then decreases when the refractive index is over 1.55. Fig. 6 (b) also accounts for the fact. For small resist indices, the period of the interference pattern decreases rapidly. This is because the period is inversely proportional to the cosine function of the resonance angle. Due to the fact that the refractive indices of all the existing resists are over 1.5, possible period variation for the interference patterns is less than 4 nm. In Fig. 6(c), we observe that the exposure depth maximum is located at around 1.53 and the exposure depth is very sensitive to large refractive index. When the refractive index of the resist is greater than 1.53, a variation of 0.4 will result in a loss of 180 nm exposure depth. However, the exposure depth is not sensitive to small refractive

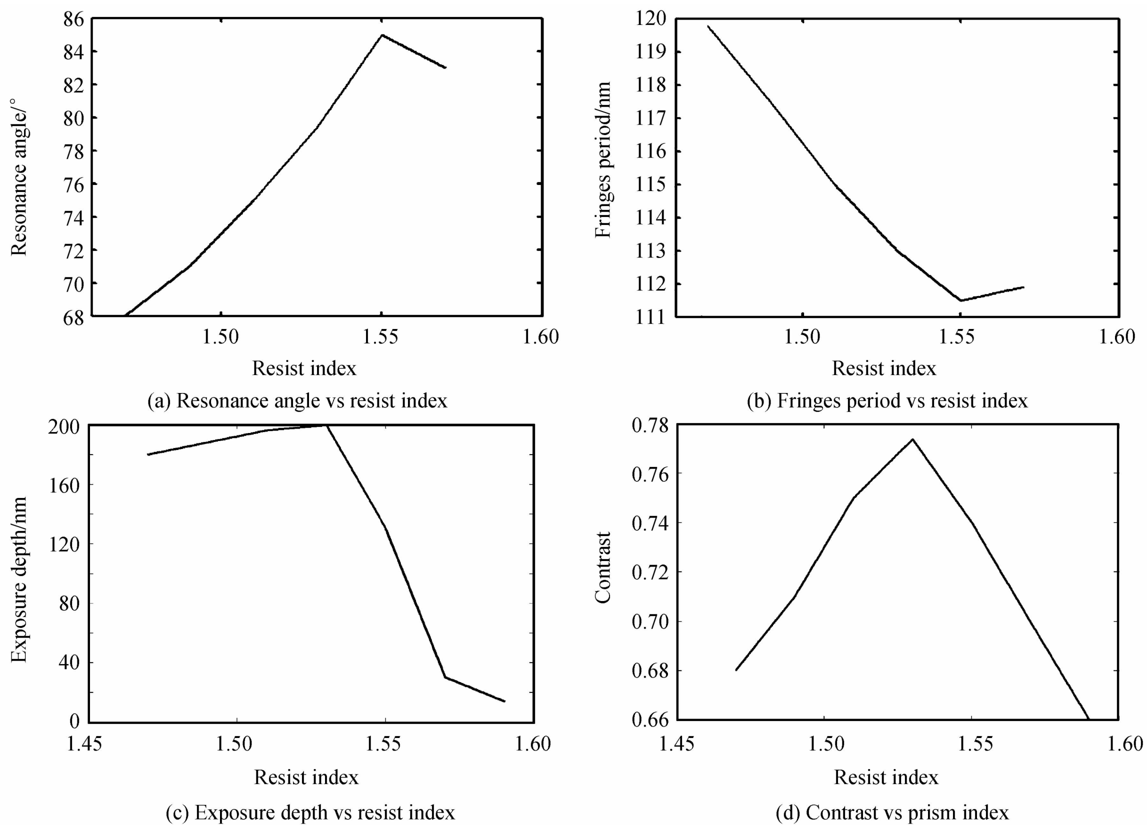

(a) Resonance angle vs resist index (b) Fringes period vs resist index

(c) Exposure depth vs resist index (d) Contrast vs prism index

Fig. 6 The resonance angle, the period, exposure depth and contrast as a function of the silver thickness

indices. From 1.5 to 1.53, the exposure depth keeps over 180 nm. The contrast of the interference pattern as a function of the resist index is shown in Fig. 6(d). The refractive index of the resist should be chosen within 1.56 to obtain more than 50 nm exposure depth. We observe that the best contrast is corresponding to the refractive index of 1.53 and the contrasts at other refractive indices decrease to some extents. All the contrasts are sufficient for lithography use.

4 Conclution

In conclusion, we numerically explore the parameter spaces used in SPP maskless lithography system. Incidence wavelength provides potential to widely change the resolution. In a simple visible light range, the period of interference pattern can vary from 110 nm to 220 nm. In this sense, SPP maskless lithography is similar to the convention photolithography. The exposure depth and pattern contrast are sensitive to the structure parameters. As a result, the structure parameters are limited in a narrow choice range in order to obtain effective interferences. When chosing 40 nm silver film at 431 nm incidence wavelength, exposure depth achieves 200 nm, and fringes period is 110 nm. It is worth pointing out that the lithography structure can be improved to obtain better lithography performance, such as the use of insulator/metal/insulator structure or metal/insulator /metal structure.

References

[1] LEVENSON M D. Extending the lifetime of optical lithography technologies with wavefront engineering [J]. *Japanese Journal of Applied Physics*, 1994, **33**(12B): 6765-6773.

[2] OKAZAKI S. Resolution limits of optical lithography [J]. *Journal of Vacuum Science & Technology*, 1991, **9**(6): 2829-2833.

[3] HAYASHI N, KURIHARA M, SEGAWA T. Electron beam lithography process for advanced optical masks[J]. *Journal of Vacuum Science & Technology*, 1998, **16**(6): 3158-3163.

[4] SPRINGHAM S V, OSIPOWICZ T, SANCHEZ J L, *et al*. Deep ion beam lithography for micromachining applications [C]. *Singapore: SPIE*, 1997, **3183**: 128-137.

[5] WILDER K, QUATE C F, SINGH B, *et al*. Electron beam and scanning probe lithography: a comparison[J]. *Journal of Vacuum Science & Technology*, 1998, **16**(6): 3864-3873.

[6] STEWART M D, JOHNSON S C, SREENIVASAN S V, *et al*. Nanofabrication with step and flash imprint lithography [J]. *Journal of Micro/Nanolithography, MEMS, and MOEMS*, 2005, **4**(1): 1-6.

[7] GOODBERLET J G, KAVAK H. Patterning Sub-50 nm features with near-field embedded-amplitude masks [J]. *Applied Physics Letters*, 2002, **81**(7): 1315-1317.

[8] LUO X, ISHIHARA T. Surface plasmon resonant interference nanolithography technique[J]. *Applied Physics Letters*, 2004, **84**(23): 4780-4782.

[9] SHAO D B, CHEN S C. Surface-plasmon-assisted nanoscale photolithography by polarized light [J]. *Applied Physics Letters*, 2005, **86**(25): 253107.

[10] GUO X, DU J, GUO Y, *et al*. Large-area surface-plasmon polariton interference lithography[J]. *Optics Letters*, 2006, **31**(17): 2613-2615.

[11] SREEKANTH K V, MURUKESHAN V M, CHUA J K. A planar layer configuration for surface plasmon interference nanoscale lithography[J]. *Applied Physics Letters*, 2008, **93**(9): 093103.

[12] DEROUARD M, HAZART J, LERONDEL G, *et al*. Polarization-sensitive printing of surface plasmon interferences[J]. *Optics Express*, 2007, **15**(7): 4238-4246.

[13] LIM Y, KIM S, KIM H, *et al*. Interference of surface plasmon waves and plasmon coupled waveguide modes for the patterning of thin film [J]. *IEEE Journal of Quantum Electronics*, 2008, **44**(4): 305-311 .

[14] MURUKESHAN V M, SREEKANTH K V. Excitation of gap modes in a metal particle-surface system for sub-30 nm plasmonic lithography[J]. *Optics Letters*, 2009, **34**(6): 845-847.

[15] XIONG W, DU J, FANG L, *et al*. 193 nm interference nanolithography based on SPP [J]. *Microelectronic Engineering*, 2008, **85**(5-6): 754-757.

[16] YANG F, SAMBLES J R, BRADBERRY W. Long-range surface modes supported by thin films[J]. *Physical Review B*, 1991, **44**(11): 5855-5872.

[17] QUAIL J C, RAKO J G, SIMON H J. Long-range surface-plasmon modes in silver and aluminum films [J]. *Optics Letters*, 1983, **8**(7): 377-379.

[18] SHAO D B, CHEN S C. Numerical simulation of surface-plasmon-assisted nanolithography[J]. *Optics Express*, 2005, **13**(18): 6964-6973.

[19] JOHNSON P B, CHRISTY R W. Optical constants of the noble metals[J]. *Physical Review B*, 1972, **6**(12): 4370-4379.

[20] LUO X G, ISHIHARA T. Subwavelength photolithography based on surface-plasmon polariton resonance [J]. *Optics Express*, 2004, **12**(14): 3055-3065.

表面等离子体无掩膜干涉光刻系统的数值分析

董启明，郭小伟

（电子科技大学 光电信息学院，成都 610064）

摘　要：表面等离子体激元具有近场增强效应，可以代替光子作为曝光源形成纳米级特征尺寸的图像．本文数值分析了棱镜辅助表面等离子体干涉系统的参量空间，并给出了计算原理和方法．结果表明，适当地选择高折射率棱镜、低银层厚度、入射波长和光刻胶折射率，可以获得高曝光度、高对比度的干涉图像．入射波长为 431 nm 时，选择 40 nm 厚的银层，曝光深度可达 200 nm，条纹周期为 110 nm．数值分析结果为实验的安排提供了理论支持．

关键词：干涉光刻；表面等离子体激元；克莱舒曼结构